Chemical Science

Accepted Manuscript

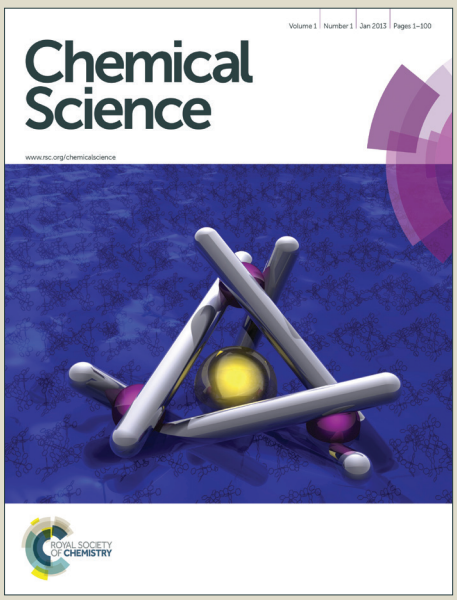

ROYAL SOCIETY OF CHEMISTRY

www.rsc.org/chemicalscience

History-dependent Ion Transport through Conical Nanopipettes and Implications in Energy Conversion Dynamics at Nanoscale Interfaces

Yan Li, Dengchao Wang, Maksim M. Kvetny, Warren Brown, Juan Liu[£] and Gangli Wang*

Department of Chemistry, Georgia State University, 50 Decatur St. SE, Atlanta, Georgia 30303

£ Current address:

Juan Liu, PhD
Department of Chemistry and Biochemistry,
University of Maryland, Baltimore County
1000 Hilltop Circle Baltimore, MD 21250

** Corresponding author:*
To whom correspondence may be addressed:
Dr. Gangli Wang, E-mail: gwang@gsu.edu Phone: 404-413-5507
Department of Chemistry, Georgia State University, P.O. Box 3965, Atlanta, Georgia 30302-3965

Keywords: Electrical Double Layer at Nanoscale, Dynamic Ion Transport at Nanoscale Interfaces, Solid-state Ion Pump, Conical Nanopore/nanopipette, Power Generation,

Abstract:

The dynamics of the ion transport at nanostructured substrate-solution interfaces plays vital roles in high-density energy conversion, stochastic chemical and biosensing, membrane separation, nanofluidics and fundamental nanoelectrochemistry. Further advancements in those applications require fundamental understanding of the ion transport at nanoscale interfaces. Understanding in the dynamic or transient transport, the key physical process involved, is limited, which contrast sharply to the widely studied steady-state ion transport features at atomic and nanometer scale interfaces. Here we report striking time-dependent ion transport characteristics at nanoscale interfaces in current-potential (I-V) measurements and theoretical analysis. First, a unique non-zero I-V cross-point and pinched I-V curves are established as signatures to characterize the dynamics of ion transport through individual conical nanopipetts. Second, ion transport against a concentration gradient is regulated by applied and surface electrical fields. The concept of ion pump or separation is demonstrated via the selective ion transport against concentration gradients through individual nanopipettes. Third, this dynamic ion transport process under predefined salinity gradient is discussed in the context of nanoscale energy conversion in, i.e. supercapacitor type charging-discharging as well as chemical and electrical energy conversions. The analysis of the emerging current-potential features establishes the urgently needed physical foundation for energy conversion employing ordered nanostructures. The elucidated mechanism and established methodology are generalizable into broadly-defined nanoporous materials and devices for improved energy, separation and sensing applications.

Introduction:

The transport of charges at solid-solution interfaces is a key step in fundamental electrochemistry,[1, 2] energy technology (i.e. charging and discharging of supercapacitors, fuel cells and batteries),[3-5] separation (i.e. desalination, filtration),[6] sensing (i.e. DNA sequencing and stochastic single molecule detection),[7-9] and natural processes in biology (i.e. ion channels and pumps) and geoscience.[10] Materials and devices with defined atomic and nanometer scale pore structures have great potentials to enhance the efficacy and/or efficiency of those applications.[11, 12] At nanoscale interfaces, novel transport phenomena emerge that require further experimental and theoretical studies. Representative features include steady-state ion current rectification (ICR),[13-15] apparent inductive behaviors,[16] mem-capacitance,[17] and 'abnormal' hysteresis and capacitance responses under high-frequency electric field stimulation[18-20] observed in different channel-type nanodevices.

The ion transport process is associated with energy conversion and characterized by current *I*, potential *V* or power (*I*V*). Recent advances in steady-state studies pave the way for better understandings of the dynamic ion transport at nanoscale interfaces, which are urgently needed to advance three types of important applications. First, ion transport through porous electrodes is the physical process and rate-limiting step in the charging and discharging of electrochemical capacitors (supercapacitors). Supercapacitors are widely used as energy device complementing or competing with batteries etc. One of the key merits of supercapacitors is that they deliver high power. The high power unfortunately leads to a major limitation: they don't last long before a recharge is needed. It is therefore highly desirable to control the power output, or the charging and discharging kinetics. Two other applications are inspired by natural processes of protein ion pumps in which chemical energy (i.e. ATP-ADP) is converted into electrochemical potential in terms of action potential, concentration gradient etc. In the second type applications, electrical energy is harvested i.e. from salinity gradient, pressure driven flow, etc. with classic ion selective membranes and recently using nanopores. Third, selective ion transport will enable ion

enrichment/depletion or separation (i.e. desalination by consumption of electricity, light, etc.).[21-29] The main limiting factors for improvements reside in the lack of fundamental physical understanding of the transport dynamics and the needs of significant enhancements in methodology

Our approach to analyze dynamic transport through solid-state nanopores in comparison to protein ion pumps is illustrated in Figure 1. A nanopore in quartz substrate allows the exchange of ions between the tip and bulk solutions. Unlike the energy from ATP hydrolysis being converted into concentration gradient, an alternating bias is applied to drive the dynamic ion transport. The time dependent I-V studies reveal dynamic transport features inaccessible in the commonly-adopted steady-state analysis. For clarification, a comparison between steady-state and dynamic/transient transport is analogous to that of uniform velocity versus acceleration/deceleration. The dynamic ion transport gains substantial contributions from the tip-localized surface electric field. Further, the salinity gradient on the two sides of the nanopore in bulk solutions is introduced. The predefined salinity gradient enables the analysis of the energy conversion between electric and chemical potential. The conversion efficiency is time dependent and characterized by power. The energy conversion efficiency or power is found to depend on previous-conductivity-state. This history-dependent feature, not captured in previous studies, enables the elucidation of drastic enhancement by surface electric field.

Highlighted in panel b inset, surface electric field has a component E_s along the direction of ion flux (or applied field) that distinguishes this asymmetric nano-geometry platform from symmetric nanochannels, and from amorphous or ensemble porous membranes. The transport limiting tip region has an orifice radius a few tens of nanometers. Correspondingly, high efficiency energy conversion is achieved in terms of nanointerface enhanced ion transport.

We first lay the foundation by introducing time-dependent hysteresis I-V features in symmetric tip:bulk concentration conditions. A unique non-zero I-V cross-point and pinched I-V loops are then employed as characteristics to evaluate the efficacy of energy conversion and pumping

ions against concentration gradient in asymmetric concentrations. Theoretical equations are developed by correlating the cross-point potential and current clamping in I-V and V-t studies respectively, through which significant surface impacts and the contributions by diffusion and migration to the overall measured current signal are elucidated. The findings are generalizable for different types of substrate-solution interfaces, therefore broadly impact the aforementioned applications.

Results and Discussion:

Dynamic I-V features from ion transport through a quartz nanopipette under symmetric tip-bulk concentrations

Representative ionic current responses of conical nanopipettes under a scanning triangular potential waveform are shown in Fig.2. The nanogeometry is analyzed by scanning electron microscope and conductivity measurements (Fig.S1). The immediate notable feature in each curve is that in the cyclic scans (scan direction shown in inset), two hysteresis loops are separated by a unique cross-point at a small positive bias rather than origin. The large hysteresis effects at such low frequency range indicate significant surface effects on pulled conical nanopipettes. Similar I-V features on a new device platform is in agreement with our recent report of pinched hysteresis loops and a non-zero cross-point in the ion transport through bench-top fabricated conical nanopores, and thus strongly supports the proposed analysis therein.[20] Such dynamic I-V features have not been observed in steady-state transport studies using broadly defined channel-type nanodevices to the best of our knowledge. To compare with steady-state responses, the non-linear I-V curve of each scan segment, specifically the current amplitude being higher at one bias than that at the opposite bias polarity, corresponds to the well-known ICR behavior.[15, 30-34] A key difference is that the I-V curve does not necessarily cross through the origin (0,0) as approximated in previous reports.

The intriguing observation of a unique non-zero I-V cross-point separating opposite hysteresis loops reveal unknown fundamental ion transport dynamics at nanoscale interfaces. In solution I-V measurements, a hysteresis loop is normally interpreted as capacitive responses. On the low conductivity side (defined as more negative bias from cross-point), ionic current displays a hysteresis corresponding to normal capacitive behavior, or positive phase shift of current responses with respect to the applied scanning potential waveform. On the high conductivity side, however, the measured current shows a hysteresis corresponding to negative phase shift, or negative capacitive responses. This negative phase shift is in agreement with the 'apparent inductive' or 'negative capacitive' behaviors reported in impedance experiments and molecular dynamic simulations on different types of nanochannel platforms respectively.[16, 17] Rooted on the steady-state ICR studies, those dynamic ion transport features observed from different nanochannel platforms have been attributed to surface electric field effects. [16-20]

Solution ionic strength is systematically varied to unveil the impacts on the hysteresis I-V features by surface electric field shown in Fig.2. On SiO_2 substrate, surface electric field originates from the negative surface charges due to the deprotonation of surface silanol groups. With the increase in KCl concentration, electrostatic interactions between mobile ions and surface charges are more effectively screened. The cross-point potential V_{cpp} decreases accordingly. The current (in general and at cross-point) increase at higher KCl concentration because more charge carriers (mobile ions) are accessible to the current-limiting nanotip region.

The cross-point can be understood as corresponding to the applied field that balances the effective surface electric field E_s across the quartz membrane at the nanotip region in potential scanning experiments (Fig.1b) explained in our early reports.[20 35] For easy perception, we use the elongation/compression of a spring as an analogy here. A spring mimics the nanopipette, with the relaxed state (length L) corresponding to the intrinsic surface charges/potential and nanogeometry. Next we consider the surface effects in ionic solution as the weight added. The

spring will elongate differently with different weights (L+W). This scenario mimics the cross-point that appears at non-zero position and depends on solution ionic strength. Without external bias, the ion distribution at the nanopipette tip region is established by the intrinsic surface electric field. The EDL at the nanointerface is at rest or unpolarized. The net ion flux or transport current is zero. Under an external bias, ion flux will alter the ion distribution, or polarize the EDL structure at the nanotip region. Accordingly, surface effects emerge and affect the measured current because the surface electric field is no longer balanced. The true steady-state, with non-zero flux/current, is established when the applied bias is equal to the effective surface potential across the nanotip.

If the spring setup is further stretched by an external force to L+W+P, (P represents the impacts by an external bias in I-V measurements), regardless of further stretching or a release by the external force, the spring setup itself will tend to recover toward L+W. Similarly, regardless if the bias is scanned in the forward or backward directions, i.e. from +0.5 V away from or toward the cross point, within one of the hysteresis loops, the surface EDL tends to recover to the rest state. In other words, the surface effects will continue to enrich the ions in high conductivity loop and deplete ions in the low conductivity loop regardless of bias scan directions. Further, because the ion flux is not zero immediately before the bias is scanned to zero, non-zero current signals are detected 'memorizing' the previous conductivity states due to the still-polarized EDL. The true steady-state is established at the cross point when the extent of the EDL polarization leads to a match in the magnitude of the surface and applied electric fields along the ion transport direction.

Steady-state ICR (i-V branch from the backward scan as a better mimic due to longer accumulation) results from the overlapping effects of the intrinsic surface electric field with respect to a constant applied electric field. Accordingly, the hysteresis effects are attributed to the differences in the kinetics of the applied potential (determined by scan rate, or frequency) with respect to the responding ion transport through the nanopipette. It is worthy pointing out

that the direction of E_s is solely determined by the surface charge polarity, albeit its magnitude varies at different ionic strength and at different applied bias because it depends on the ionic distribution at the nanotip. Therefore, at a bias more positive than the cross-point, the surface field consistently facilitates ion transport driven by the applied field regardless of the respective magnitudes, thereby reducing resistance and cause negative capacitance, correspondingly the high conductivity states and negative I-V hysteresis.

This non-zero cross-point is employed as a signature in the following discussions because it is stable and unique for each measurement system (Figs. S2-S4). At each scan rate, the I-V curves from multiple scans overlap with the variation in cross-point within 5 mV (the first or few segment/s are discarded to better present stable I-V responses). This variation is acceptable within experimental errors such as imperfect Ag/AgCl electrodes preparation, thermo agitation and external interference etc. The I-V features are also found independent of initial potential or initial scan directions. A small variation in cross-point potential could be observed at less than 10 mV at different scan rates employed in this report. This variation intensified at higher scan rates, which has been attributed to the charging and discharging of quartz substrate (through exterior interfaces).[35] The effect is ignored in the following discussion because it is insignificant with regards to the trend discussed in this report.

Dynamic ion transport through a quartz nanopipette under asymmetric tip:bulk concentrations

Next we analyze the dynamic ion transport under a concentration gradient across the nanopore driven by an external bias. A series of I-V curves using a single nanopipette in asymmetric tip:bulk KCl concentrations are presented in Fig. 3. The feature near the cross-points can be seen in the insets. Similar trends were obtained from different nanopipettes (Fig.S5). Systematic

studies using the same nanopipette eliminate the impacts by possible imperfection in nanodevice geometry, particularly the transport-limiting nanotip interior portion that could not be directly characterized. Because the nanopipette geometry remains constant in those measurements, geometric impacts can be deconvoluted. The approach enables direct correlation of the transport features with surface charge effects, which has been a long standing challenge to study due to the heterogeneous nature of surface charge distribution, particularly at nanoscale interfaces. As a reminder, surface effects are known to be significant and even determinant factors in the ion transport processes through various channel-type nanodevices.

The cross-points of those systematic concentration combinations are summarized in Fig.4. Because the two Ag/AgCl wires are soaked in different KCl concentrations, unlike those in the same KCl solution, the potential drop at the two electrode–solution interfaces does not cancel each other and needs to be corrected. The net redox potential is described by Nernst expression (V_{redox}). The total bias at the cross-point ($V_{CPP(i\text{-}V)}$) therefore includes V_{redox} and V_{pore} (the potential drop across the nanopore) as expressed in Eq. 1. V_{pore} includes both surface field and concentration gradient effects discussed next.

$$V_{CPP\ (i-V)} = V_{pore} + V_{redox} = V_{pore} + \frac{RT}{F}\ln\frac{K_{sp\ AgCl}/a_{bulk\ KCl}}{K_{sp\ AgCl}/a_{tip\ KCl}} \quad (1)$$

in which the activity of Ag^+ (a_{Ag^+}) is approximated as concentration, which is inversely proportional to that of Cl^-. R is gas constant, T is temperature and F is Faraday's constant.

At each specific tip concentration, an increase in bulk concentration will cause V_{pore} (or the measured V_{cpp}) to shift toward more negative bias. At each specific bulk concentration, an increase of tip concentration will cause positive-shift of V_{pore}. The data also suggest that comparable concentration gradients induce similar shift magnitudes of V_{cpp}. At even higher concentration gradients, the cross-points could deviate from the trend presented in Fig.4

(Shown in Fig.S6 a&b). The deviation might be associated with the challenges to establish stable and controllable concentration gradient, which is a prerequisite for this report.

With the increase of bulk or tip KCl concentrations, the current increase due to the increase of accessible charge carriers on either side of the transport-limiting nanotip region. The cross-point current is more sensitive to the tip concentration and to a lesser extent the bulk. This is because the measured current is primarily limited by a segment inside the nanopipette orifice. The current data at +/- 1V of each curve are listed in Table S1. Further current analysis requires surface charge parameters at the nanotip that are known to be heterogeneous and thus unavailable for individual nanodevices. This is being addressed in a combined experimental and simulation study underway.

Balance of diffusion and migration flux by zero current clamping

Under the low potential amplitude and other experimental conditions employed here, ion flux arises primarily from 1. diffusion determined by concentration gradient and 2. migration regulated by both applied and surface electric fields.[31, 32, 36] The measured current signals reflect the net ion flux limited by the nanotip region. Chronopotentiometry is employed next to elucidate the respective ion flux contributions by migration and diffusion. The applied potential is recorded over time till it reaches a stable value $V_{rev\ (i\text{-}t)}$, during which the measured current is clamped to zero. This corresponds to no net flux of charges through the pore. In other words, at zero current, the ion flux driven by the external bias balances that by the concentration gradient. As expected in symmetric tip-bulk concentration conditions, the diffusion potential V_{diff} is zero (within experimental error at few millivolts). Analogous to the cross-point potential analysis in I-V studies, the reversal potential V_{rev} includes V_{redox} in addition to the diffusion potential as expressed in equation (2).

$$V_{rev\,(i-t)} = V_{diff} + V_{redox} = (t_+ - t_-)\frac{RT}{F}\ln\frac{a_{tip\,KCl}}{a_{bulk\,KCl}} + \frac{RT}{F}\ln\frac{a_{tip\,KCl}}{a_{bulk\,KCl}} = 2t_+V_{redox}$$

(2)

This quantitative correlation is affirmed by the nice linear fitting of the measured V_{rev} versus theoretical V_{redox} shown in Fig. 5 (a). The V_{rev} values and representative V-t curves are included in Fig. S7 and Table S2. From the slope, cation transference number is determined to be 0.69 for this nanopipette. Since ion selectivity is a significant parameter in membranes for i.e. desalinization, and broadly defined separation science and energy technologies, it is exciting for this analysis to directly characterize cation selectivity of a single nanopore experimentally. Because K^+ and Cl^- mobility is comparable, no diffusion potential is expected in bulk solution (transference number at 0.5 each). The large cation transference number reflects surface electric field effect, which induces asymmetric cation and anion diffusional flux and makes this nanodevice cation-selective. The correlation in equation (2) is further validated by the results from different nanopipettes analyzed in Fig. S8. The variation in those t_+ values suggests heterogeneous surface charge effects of individual nanopipettes.

In our earlier studies based on conical nanopore platform in symmetric concentrations, the effective transmembrane potential V_M was found to depend on the electrolyte concentrations by a square root function. In the expression shown as the last portion in equation (3), analogous to the Debye length description in classic double layer theory, V_0, A, V_e correspond to surface potential inside nanotip, a constant that is temperature dependent, and non-ideal factors associated with measurements respectively.[20]

$$V_{CPP\,(i-V)} - V_{rev\,(i-t)} = V_{pore} - V_{diff} = V_{M\,(i-V)} = V_0\exp(-\frac{C_{KCl}^{1/2}}{A}) + V_e \quad (3)$$

A correlation of I-V and I-t measurements by equation (3) will reveal nanointerface parameters such as surface potential (V_0). Subtraction of V_{redox} from both types of measurements reveals

the potential drop at the nanotip region (bulk-to-tip across the quartz membrane). At each tip concentration, V_M from symmetric tip:bulk concentrations matches that by the elimination of the diffusion potential in asymmetric concentrations (i.e. at 5 mM tip conc., 108 mV – 63 mV = 45 mV at 5:1 ratio matches the 50 mV at 5:5 ratio within ± 5 mV). The analysis suggests that the tip concentration plays more significant roles in the transport measurements (data listed in Table S2). The linear correlation in Fig.5 strongly supports the correlation of equation (3). The scattering at different bulk concentrations is attributed to the variation of local concentration gradients in different measurements. The concentration range in this study is adopted to ensure stable and reproducible concentration gradients. With predefined salinity and salinity gradient, this analysis offers the full picture of dynamic ion transport across an asymmetric nanopore influenced by diffusion and migration.

Implications on selective ion transport and history-dependent energy conversion at nanointerfaces

Three key factors have been correlated in this time-dependent ion transport analysis: the applied electric field, surface electric field, and salinity gradient. Each cross-point is at a unique balance of the three factors in the corresponding current-potential analysis.

Selective ion transport and ion pumping

The intrinsic ion selectivity (no bias applied) of a negatively charged nanopore can be characterized by the aforementioned analysis of cation transference number. At a bias more negative than the cross-point potential, low conductivity zone is established. The depletion of anion transport makes this zone highly cation selective due to negative surface charges. This is supported by cation transference number approaching unity in earlier simulation and experimental studies. [37-39] The high conductivity zone, at the bias more positive than the cross point, is associated with high ionic strength and thus a decrease in ion selectivity. [37-39] Therefore,

high conductivity region is more favorable for energy conversion applications (high power) rather than separation.

To relay to the ion pump concept, the cross-points in Fig.4 can be divided into three categories: $C_{tip} = C_{bulk}$, $C_{tip} < C_{bulk}$, and $C_{tip} > C_{bulk}$. The transport of cation is considered because it constitutes the majority of the measured current signal. For $C_{tip} < C_{bulk}$, cations are pumped against their concentration gradient at low conductivity side, driven by applied potential but inhibited by surface potential. On high conductivity side, cations move along the concentration gradient, and thus no pumping effect. For $C_{tip} > C_{bulk}$, cations are pumped against their concentration gradient at high conductivity side, driven by applied potential and facilitated by surface potential. At low conductivity side, no pumping effect is expected. Four representative scenarios illustrate the physical picture of the corresponding transport processes (Fig. S9). For applications that require anion selectivity, positively charged surfaces can be created, by i.e. chemical modification, to enable favorable transport of anion over cation. The same principles apply to different salinity gradients.

History-dependent energy conversion at nanointerfaces

Cross-point signature At the cross-point, steady-state ion flux is established by the three factors: the current and potential at the cross-point indicate the external power/energy input required to balance the surface electrical field effects, plus the salinity gradient if adopted. Thus, the product of I*V at the cross-point represents the natural capacity of the employed nanointerface for the energy conversion process. The I(t)*V(t) at cross-point is referred as power P_{cpp}. To evaluate the energy conversion or power in conventional electronic circuits, open-circuit-potential (OCP) and short-circuit-current (SCC) are routine analysis because the triangular area in the I-V plots represents the max power (for a simple resistor load, $P=I*V=I^2*R=V^2/R$). Similar analysis has been adopted to evaluate the maximum power of various nanochannels under

salinity gradient.[4, 22, 24] It is important to realize that P=I*V=0 in either OCP or SCC conditions ($I_{V=0}$ times $V_{I=0}$ evaluation). Therefore, caution should be taken in the nanopore systems because their resistance and capacitance vary and depend on the transport dynamics. Therefore, we propose P_{cpp} as a parameter with more rigorously defined physical meaning in the evaluation of transport related energy conversions at nanointerfaces, especially in systems with prominent rectification and hysteresis.

Power analysis and comparison Importantly, P_{cpp} values are comparable in magnitudes with the products of $I_{V=0}$ times $V_{I=0}$ for different nanopipettes, and comparable in general with those in related literature for power generation under salinity gradients (Table S3).[40] Unlike those literature studies performed in high pH conditions to induce higher surface effects, our measurements were performed in ambient pH to avoid the introduction of different types of ions that complicates the mechanism elucidation. Therefore, we expect further enhancement in the already-impressive power of our system at higher pH and/or high salinity gradient conditions.

Hysteresis in the charging-discharging kinetics History-dependent energy conversion is illustrated in Fig. 6. The following discussion is focused on high conductivity states that are better suited for energy applications. In reference to the volumetric conductance, drastic surface effects can be quantified at different time or bias domains. For example, at 0.60 V, $I(t_b)$ is larger than $I(t_f)$ due to the longer period during which larger surface effects accumulate (sustained contribution by E_s). Similarly, both forward and backward currents are lower at higher scan rates due to less surface enhancement over shorter time at the same potentials. This surface enhancement functions regardless of salinity gradients. Given the P_{cpp} describes the intrinsic capacity of individual nanostructures for power generation under salinity gradient and establishes the physical meaning of such power generation under an external bias, further enhancement by the nanointerface in the power generation is anticipated if a positive bias were applied. The concept is analogous to the gain effect in field effect transistors. Further, the

forward and backward scans correspond to charging and discharging of the nano-supercapacitor respectively. The hysteresis therefore suggests a delay in the charging (forward scan) as well as discharging (backward scan) driven by the external potentiostat. In other words, asymmetric nanopore structures and local surface electric field effects will alter the kinetics of energy conversion. Our analysis suggests that, theoretically, the time constants of the energy conversion could be tuned by engineering nanointerfaces to achieve desired power input-output for specific energy storage, power generation and other related applications.

Conclusions:

To summarize, time-dependent current potential features of individual conical nanopipettes are studied through which fundamental understanding in dynamic ion transport at nanoscale interfaces is established. Employing salinity gradient across a conical quartz nanopipette, hysteresis in the ion transport current with respect to a stimulating alternating electrical field is characterized by a non-zero I-V point and pinched I-V loops. The product of I-V, i.e. power at the unique cross-point is shown to be a more accurate and meaningful signature to characterize the dynamic ion transport or energy conversion at individual nanodevices. The hysteresis effect in I-V measurements has significant implications on the charging-discharging kinetics of energy devices such as supercapacitors. Further, the conversion of salinity gradient into electrical energy, or vice versa, on asymmetric conical nanopore platform is demonstrated to be enhanced drastically by an intrinsic surface electrical field. The prerequisites to observe such time-dependent transport features and possible routes for further optimization are the asymmetry, such as the nanogeometry and fixed surface charges, for the ions to experience within the time frame of stimulus or measurements. The findings suggest exciting opportunities to advance energy, separation and other related applications using broadly-defined channel-type nanodevices. The theoretical foundation and analysis methodology are universal and

generalizable to other structurally-defined nanoporous materials and nanodevices, and thus believed applicable in broad energy and separation applications.

Methods and Materials:

Quartz nanopipettes were fabricated with P-2000 puller (Sutter Instrument Co.) using quartz capillaries (O.D.:1.0 mm, I.D.: 0.7 mm). The pulling parameters of the nanopipettes are as follows: Heat: 700, Filament: 4, Velocity: 60, Del: 150, Pull: 120. The experiments were performed with Gamry Reference 600 (Gamry Co.). Two Ag/AgCl wires were used as electrodes. One was immersed inside of the nanopipette as reference electrode while the other one in the bulk solution as working electrode. Bias is therefore defined as outside versus inside. The current was recorded under an applied triangular potential waveform at 100 mV/s scan rate. The reported stable I-V curves were recorded after discarding the first few I-V segments and confirmed by the overlap of last five scans. To ensure the designed concentration gradient, the nanopipette will be centrifuged ca. 20 min after replacing the tip solution. Reproducible I-V responses in symmetric setups were recorded between each asymmetric study to affirm the proper concentrations being used. After each set of I-V measurements with same tip concentration, additional I-V measurements under at least one asymmetric condition were conducted to demonstrate stability and reproducibility of the measurements.

Acknowledgements

The support by NSF under Grant No. 1059022 is acknowledged. The contributions by DW and GW are partially supported as part of the Fluid Interface Reactions, Structures and Transport

(FIRST) Center, an Energy Frontier Research Center funded by the U.S. Department of Energy, Office of Science, Office of Basic Energy Sciences.

Notes and references:

1. A. J. Bard and L. R. Faulkner, *Electrochemical methods : fundamentals and applications*, Wiley, New York, 2001.
2. S. M. Oja, M. Wood and B. Zhang, *Anal. Chem.*, 2013, 85, 473.
3. R. B. Schoch, J. Han and P. Renaud, *Rev. Mod. Phys.*, 2008, 80, 839.
4. W. Guo, L. X. Cao, J. C. Xia, F. Q. Nie, W. Ma, J. M. Xue, Y. L. Song, D. B. Zhu, Y. G. Wang and L. Jiang, *Adv. Funct. Mater.*, 2010, 20, 1339.
5. J. W. Long, B. Dunn, D. R. Rolison and H. S. White, *Chem. Rev.*, 2004, 104, 4463.
6. B. E. Logan and M. Elimelech, *Nature*, 2012, 488, 313.
7. J. Clarke, H. C. Wu, L. Jayasinghe, A. Patel, S. Reid and H. Bayley, *Nat. Nanotechnol.*, 2009, 4, 265.
8. M. Zwolak and M. Di Ventra, *Rev. Mod. Phys.*, 2008, 80, 141.
9. D. Branton, D. W. Deamer, A. Marziali, H. Bayley, S. A. Benner, T. Butler, M. Di Ventra, S. Garaj, A. Hibbs, X. Huang, S. B. Jovanovich, P. S. Krstic, S. Lindsay, X. S. Ling, C. H. Mastrangelo, A. Meller, J. S. Oliver, Y. V. Pershin, J. M. Ramsey, R. Riehn, G. V. Soni, V. Tabard-Cossa, M. Wanunu, M. Wiggin and J. A. Schloss, *Nat. Biotechnol.*, 2008, 26, 1146.
10. A. E. S. Van Driessche, L. G. Benning, J. D. Rodriguez-Blanco, M. Ossorio, P. Bots and J. M. García-Ruiz, *Science*, 2012, 336, 69.
11. C. Dekker, *Nat. Nanotechnol.*, 2007, 2, 209.
12. C. R. Martin and Z. S. Siwy, *Science*, 2007, 317, 331.
13. Z. S. Siwy and S. Howorka, *Chem. Soc. Rev.*, 2010, 39, 1115.
14. H. Daiguji, *Chem. Soc. Rev.*, 2010, 39, 901.
15. C. Wei, A. J. Bard and S. W. Feldberg, *Anal. Chem.*, 1997, 69, 4627.
16. J. Feng, J. Liu, B. Wu and G. Wang, *Anal. Chem.*, 2010, 82, 4520.
17. M. Krems, Y. V. Pershin and M. Di Ventra, *Nano Lett.*, 2010, 10, 2674.
18. J. P. Guerrette and B. Zhang, *J. Am. Chem. Soc.*, 2010, 132, 17088.
19. D. Momotenko and H. H. Girault, *J. Am. Chem. Soc.*, 2011, 133, 14496.
20. D. Wang, M. Kvetny, J. Liu, W. Brown, Y. Li and G. Wang, *J. Am. Chem. Soc.*, 2012, 134, 3651.
21. H. Zhang, X. Hou, L. Zeng, F. Yang, L. Li, D. Yan, Y. Tian and L. Jiang, *J. Am. Chem. Soc.*, 2013.
22. J. Cervera, P. Ramirez, S. Mafe and P. Stroeve, *Electrochim. Acta*, 2011, 56, 4504.
23. W. Guo, Y. Tian and L. Jiang, *Acc. Chem. Res.*, 2013, 46, 2834.
24. A. Siria, P. Poncharal, A.-L. Biance, R. Fulcrand, X. Blase, S. T. Purcell and L. Bocquet, *Nature*, 2013, 494, 455.
25. E. C. Yusko, R. An and M. Mayer, *ACS Nano*, 2010, 4, 477.
26. Z. Siwy, I. D. Kosińska, A. Fuliński and C. R. Martin, *Phys. Rev. Lett.* 2005, 94, 048102.
27. D.-K. Kim, C. Duan, Y.-F. Chen and A. Majumdar, *Microfluidics and Nanofluidics*, 2010, 9, 1215.
28. W. Guan and M. A. Reed, *Nano Lett.*, 2012, 12, 6441.
29. F. H. J. van der Heyden, D. J. Bonthuis, D. Stein, C. Meyer and C. Dekker, *Nano Lett.*, 2006, 6, 2232.
30. S. Umehara, N. Pourmand, C. D. Webb, R. W. Davis, K. Yasuda and M. Karhanek, *Nano Lett.*, 2006, 6, 2486.

31. H. S. White and A. Bund, *Langmuir*, 2008, 24, 2212.
32. C. Kubeil and A. Bund, *J. Phys. Chem. C*, 2011, 115, 7866.
33. D. Woermann, *Phys. Chem. Chem. Phys.*, 2003, 5, 1853.
34. Z. Siwy and A. Fulinski, *Phys. Rev. Lett.*, 2002, 89.
35. D. Wang, J. Liu, M. Kvetny, Y. Li, W. Brown and G. Wang, *Chem. Sci.*, 2014, 5, 1827
36. J. Liu, D. Wang, M. Kvetny, W. Brown, Y. Li and G. Wang, *Langmuir*, 2013, 29, 8743.
37. J. Jorne, *Nano Lett.*, 2006, 6, 2973.
38. J. Liu, M. Kvetny, J. Feng, D. Wang, B. Wu, W. Brown and G. Wang, *Langmuir*, 2012, 28, 1588.
39. J. Cervera, B. Schiedt, R. Neumann, S. Mafe and P. Ramirez, *J. Chem. Phys.*, 2006, 124, 104706.
40. J. Liu; D. Wang, M. Kvetny, W. Brown, Y. Li, G.Wang, *Anal. Chem.*, 2012, 84(16), 6926.

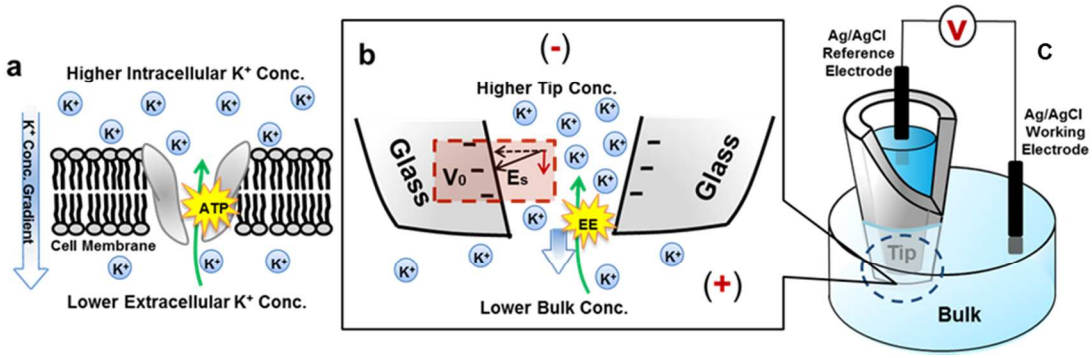

Fig. 1. Scheme of a nanopore in transmembrane protein and solid state nanopipette under ion concentration gradient. **a)** A K^+ ion pump in lipid bilayer that transports K^+ against concentration gradient by ATP hydrolysis. **b)** Enlarged view of nanopipette tip under high-tip-low-bulk concentration gradient. Quartz/Glass serves as the counterpart of the insulating lipid bilayer. K^+ ions could migrate against concentration gradient driven by external electrical energy (**EE**). Cl^- ions are omitted due to lower contribution to the ion flux as a result of repulsion from negative surface charges. Surface potential V_0 and the direction of the surface electric field E_s are highlighted. **c)** Experimental setup. The bias is defined as bulk versus tip.

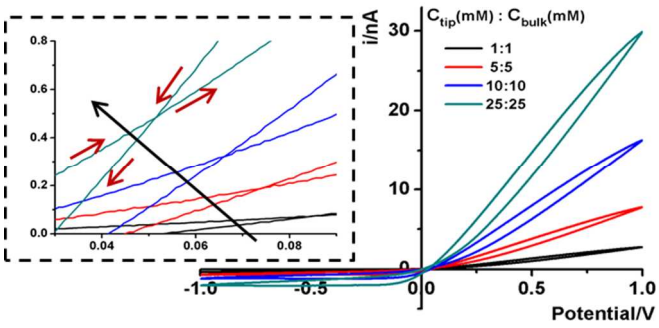

Fig. 2. Representative I-V features of a 60-nm-radius nanopipette in symmetric tip:bulk KCl concentrations. Scan rate is 100 mV/s. Inset shows the scan directions and the cross-point position of all I-V curves. The shift in cross-point with the increase of concentration is indicated by the long arrow.

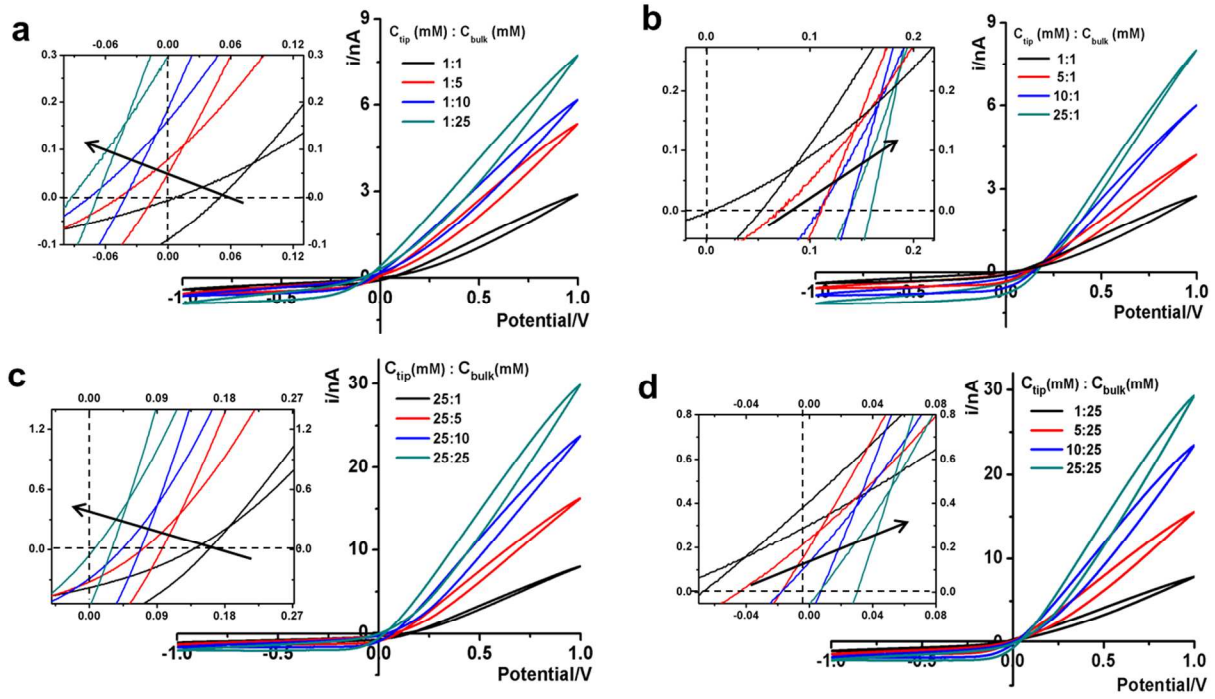

Fig. 3. Trends of I-V features in asymmetric tip:bulk KCl concentrations. The I-V curves of the 60-nm-nanopipette in the denoted C_{tip}:C_{bulk} concentration combinations: **a)** common low tip conc. **b)** common low bulk conc. **c)** common high tip conc. **d)** common high tip conc. Scan rate at 100 mV/s. Inset shows the shift in the cross-point w.r.t. the origin (0,0). Each curve was collected after multiple scans until the last five repeated scans overlapped, affirming a stable concentration gradient being established.

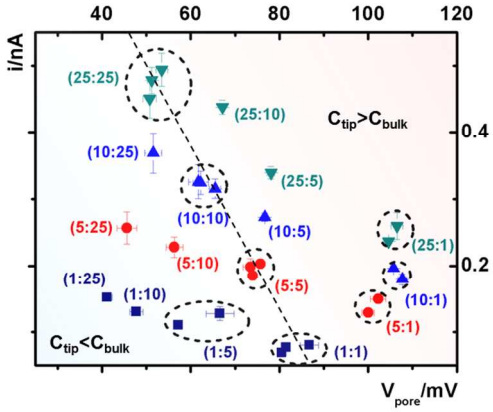

Fig. 4. Analysis of potential-corrected cross-point under designed tip:bulk concentration gradient combinations. Error bars on each point show the standard deviations from five repeated scans under each condition. Between each asymmetric concentration measurement, symmetric ones with the same tip concentration were measured to validate the efficacy in loading and replacing the solutions, particularly inside the tip. Data from repeated measurements in the same concentration combinations (both symmetric and representative asymmetric) are circled to highlight the reproducibility of the measurements.

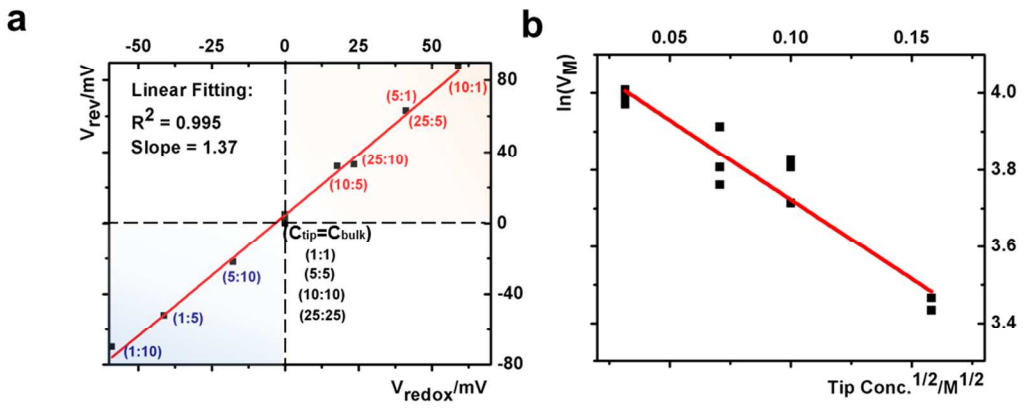

Fig. 5. a) Correlation between the measured reversal potential and the redox potential. **b)** Correlation between the corrected transmembrane potential with square root electrolyte concentration.

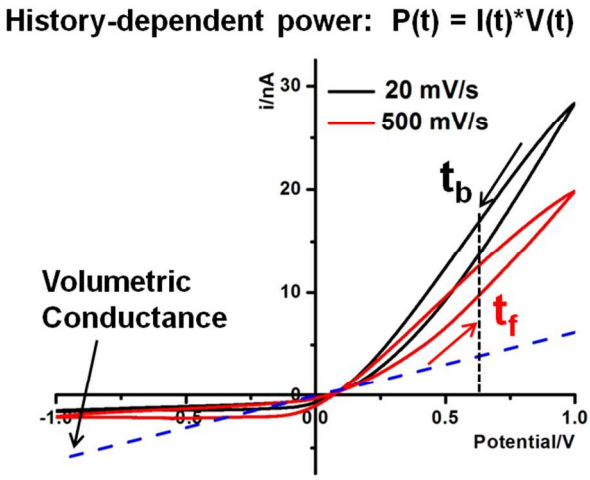

Fig. 6. History-dependent power generation of the 60-nm nanopipette in 25:10 tip:bulk concentrations at 20 mV/s and 500 mV/s. Volumetric conductance is estimated from tip concentration volumetric ohmic behaviors (blue dash line). The arrows near the current curves indicate the direction of the sweeping bias. Forward and backward scans are defined as away and toward the cross-point respectively.

FOR TOC